

Article

## Improvement of H<sub>2</sub>S Sensing Properties of SnO<sub>2</sub>-Based Thick Film Gas Sensors Promoted with MoO<sub>3</sub> and NiO

Soo Chool Lee <sup>1,†</sup>, Seong Yeol Kim <sup>1,†</sup>, Byung Wook Hwang <sup>1</sup>, Suk Yong Jung <sup>1</sup>, Dhanusuraman Ragupathy <sup>2</sup>, In Sung Son <sup>3</sup>, Duk Dong Lee <sup>4</sup> and Jae Chang Kim <sup>1,\*</sup>

<sup>1</sup> Department of Chemical Engineering, Kyungpook National University, Daegu 702-701, Korea; E-Mails: soochool@knu.ac.kr (S.C.L.); ksy256@naver.com (S.Y.K.); a048042@knu.ac.kr (B.W.H.); ojhyt@hanmail.net (S.Y.J.)

<sup>2</sup> Centre for Research & Development, PRIST University, Puducherry 605 007, India; E-Mail: ragupathypdy@prist.ac.in

<sup>3</sup> HKC, Sucho-gu, Seoul 130-070, Korea; E-Mail: hkc1959@hkci.co.kr

<sup>4</sup> School of Electrical Engineering and Computer Science, Kyungpook National University, Daegu 702-701, Korea; E-Mail: ddlee@knu.ac.kr

<sup>†</sup> These authors contributed equally to this work.

\* Author to whom correspondence should be addressed; E-Mail: kjchang@knu.ac.kr; Tel.: +82-53-950-5622; Fax: +82-53-950-6615.

Received: 29 January 2013; in revised form: 4 March 2013 / Accepted: 15 March 2013 /

Published: 19 March 2013

**Abstract:** The effects of the SnO<sub>2</sub> pore size and metal oxide promoters on the sensing properties of SnO<sub>2</sub>-based thick film gas sensors were investigated to improve the detection of very low H<sub>2</sub>S concentrations (<1 ppm). SnO<sub>2</sub> sensors and SnO<sub>2</sub>-based thick-film gas sensors promoted with NiO, ZnO, MoO<sub>3</sub>, CuO or Fe<sub>2</sub>O<sub>3</sub> were prepared, and their sensing properties were examined in a flow system. The SnO<sub>2</sub> materials were prepared by calcining SnO<sub>2</sub> at 600, 800, 1,000 and 1,200 °C to give materials identified as SnO<sub>2</sub>(600), SnO<sub>2</sub>(800), SnO<sub>2</sub>(1000), and SnO<sub>2</sub>(1200), respectively. The Sn(12)Mo5Ni3 sensor, which was prepared by physically mixing 5 wt% MoO<sub>3</sub> (Mo5), 3 wt% NiO (Ni3) and SnO<sub>2</sub>(1200) with a large pore size of 312 nm, exhibited a high sensor response of approximately 75% for the detection of 1 ppm H<sub>2</sub>S at 350 °C with excellent recovery properties. Unlike the SnO<sub>2</sub> sensors, its response was maintained during multiple cycles without deactivation. This was attributed to the promoter effect of MoO<sub>3</sub>. In particular, the Sn(12)Mo5Ni3 sensor developed in this study showed twice the response of the Sn(6)Mo5Ni3 sensor,

which was prepared by  $\text{SnO}_2(600)$  with the smaller pore size than  $\text{SnO}_2(1200)$ . The excellent sensor response and recovery properties of  $\text{Sn}(12)\text{Mo}5\text{Ni}3$  are believed to be due to the combined promoter effects of  $\text{MoO}_3$  and  $\text{NiO}$  and the diffusion effect of  $\text{H}_2\text{S}$  as a result of the large pore size of  $\text{SnO}_2$ .

**Keywords:** sensor;  $\text{SnO}_2$ ; pore size;  $\text{H}_2\text{S}$ ;  $\text{MoO}_3$ ;  $\text{NiO}$

---

## 1. Introduction

Hydrogen sulfide ( $\text{H}_2\text{S}$ ) is an unwanted and toxic by-product of the coal, coal oil, and natural gas industries [1]. When hydrogen sulfide is emitted into the atmosphere, it is converted to  $\text{SO}_x$ , which is a precursor to acid rain [2]. Accordingly, there is increasing demand for sensing devices that monitor low  $\text{H}_2\text{S}$  concentrations. Well-known materials used to detect  $\text{H}_2\text{S}$  include  $\text{BaTiO}_3$  [3],  $\text{SnO}_2\text{-Pd}$  [4],  $\text{Ag-SnO}_2$  [5],  $\text{SnO}_2\text{-Al}_2\text{O}_3$  [6],  $\text{SnO}_2\text{-CuO}$  [7–11],  $\text{SnO}_2\text{-CuO-SnO}_2$  [12,13],  $\text{SnO}_2\text{-ZnO-CuO}$  [14] and  $\text{SiO}_2$ -doped  $\text{Cu-Au-SnO}_2$  [15]. Among the sensors described in the literature,  $\text{CuO}$ -modified thin-film or thick-film  $\text{SnO}_2$  sensors are promising for the sensitive and selective detection of  $\text{H}_2\text{S}$  [1].

$\text{SnO}_2$ -based thick-film gas sensors have been used to detect toxic gases [16–28] on account of their high sensor response, simple design, low weight and low price.  $\text{SnO}_2$ -based thick film gas sensors can achieve greater sensitivity to  $\text{H}_2\text{S}$  through control of the particle size [17] and the addition of suitable promoters [13,14]. Wagh *et al.* reported that  $\text{SnO}_2\text{-ZnO-CuO}$  thick-film sensors had significantly better response and recovery times than  $\text{SnO}_2\text{-ZnO}$  or  $\text{CuO}$  doped  $\text{SnO}_2$  sensors [15]. Nevertheless, most studies on the sensing behavior of  $\text{CuO}$ -modified  $\text{SnO}_2$  thick-film gas sensors focused on concentrations of tens to hundreds of ppm. Until now, there have been very few studies of  $\text{SnO}_2$ -based gas thick-film sensors for the detection of <1 ppm  $\text{H}_2\text{S}$ .

In our previous papers, we described a  $\text{SnO}_2$ -based thick-film gas sensor promoted with  $\text{MoO}_3$  and  $\text{NiO}$ , which was developed for the detection of dimethyl methylphosphonate (DMMP) and dichloromethane [26–28]. During the course of this earlier study,  $\text{NiO}$  and  $\text{MoO}_3$  promoters were found to play important roles in the sensor response and the recovery of the  $\text{SnO}_2$ -based sensor, respectively, for the detection of toxic organic compounds containing P and Cl [26–28]. In the case of  $\text{H}_2\text{S}$  detection, a  $\text{SnO}_2$ -based thick-film sensor promoted with  $\text{NiO}$  and  $\text{MoO}_3$  showed improved recovery properties [2]. Nevertheless, the response of this sensor was decreased by promoting  $\text{MoO}_3$  despite the good recovery properties. Considering that the sensor response is an important factor in addition to the recovery properties, the improvement in the sensor response is necessary to develop a new  $\text{SnO}_2$ -based thick-film gas sensor for the detection of <1 ppm  $\text{H}_2\text{S}$ .

The aim of this study was to improve the response of a  $\text{SnO}_2$ -based thick-film gas sensor promoted with  $\text{NiO}$  and  $\text{MoO}_3$  developed in a previous study for the detection of  $\text{H}_2\text{S}$  at concentrations of <1 ppm. Accordingly, this study examined the effects of promoters and the textural properties of  $\text{SnO}_2$  on the sensing behaviors of  $\text{SnO}_2$ -based thick-film sensors.

## 2. Experimental Section

### 2.1. Preparation of the Materials and Sensors

The  $\text{SnO}_2$  used as a source for the  $\text{SnO}_2$ -based sensors was prepared from  $\text{SnCl}_4$  using a previously described ammonia-based precipitation method [2,26–28]. The products were calcined in a muffle furnace at various temperatures (600, 800, 1,000 or 1,200 °C). The  $\text{SnO}_2$ -based materials were prepared by physically mixing two or three of the following promoters,  $\text{NiO}$ ,  $\text{ZnO}$ ,  $\text{MoO}_3$ ,  $\text{CuO}$  and  $\text{Fe}_2\text{O}_3$ , with  $\text{SnO}_2$ . All products were calcined in a muffle furnace at 600 °C for 4 hours. The temperature ramp rate was 3 °C/min. The thick-film sensors were fabricated on an alumina substrate by screen-printing using a variety of physical mixtures, such as a  $\text{SnO}_2$ -based powder and an organic binder (90%  $\alpha$ -terpineol, Aldrich) [2,26–28]. The printed thick-film sensors were dried and calcined at 600 °C for 1 hour. This paper describes the sensors as  $\text{SnO}_2(600)$  or  $\text{Sn}(6)\text{Mo}5\text{Ni}3$ , where (600) represents the calcination temperature,  $\text{Sn}(6)$  represents  $\text{SnO}_2$  calcined at 600 °C, Mn5 and Ni3 represent 5%  $\text{MoO}_3$  and 3%  $\text{NiO}$ , respectively, on a weight/weight basis.

### 2.2. Sensor Testing System

The sensing behaviors were examined in a flow system equipped with a 0.1 L chamber. The  $\text{H}_2\text{S}$  gas was diluted with dry air to a concentration of <4.0 ppm. The total flow rate of the gas mixture was 400 mL/min.  $\text{H}_2\text{S}$  gas was injected into chamber for 10 minutes. In the present study, the sensor response was defined using the following equation:

$$\text{Sensor response (\%)} = [(R_a - R_g)/R_a] \times 100 \quad (1)$$

where  $R_a$  and  $R_g$  are the electric resistance in air and test gas, respectively. The sensor recovery was defined by the following equation:

$$\text{Recovery (\%)} = [(S_m - S_r)/S_m] \times 100 \quad (2)$$

where  $S_m$  and  $S_r$  represent the maximum sensor response over a period of 10 minutes and the minimum sensor response in air, respectively.

### 2.3. Characterization of Materials

The crystalline phases in the materials were identified by power X-ray diffraction (XRD; Philips, X'PERT) using  $\text{Cu K}\alpha$  radiation. The morphology of the  $\text{SnO}_2$  powder was observed by transmission electron microscopy (TEM; Hitachi, H-7100), and the textural properties of the materials were examined using an Hg porosimetry (Micromeritics, AutoPore IV 9500).

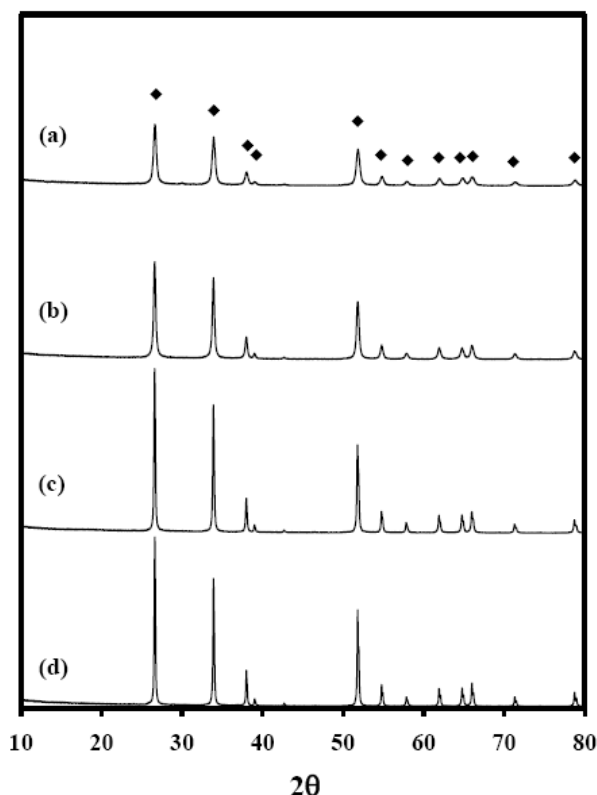
## 3. Results and Discussion

### 3.1. Effects of $\text{SnO}_2$ Pore Size on Sensor Properties

To examine the effects of the textural properties of  $\text{SnO}_2$  on the sensing properties, the  $\text{SnO}_2$  materials were prepared by calcining  $\text{SnO}_2$  at temperatures of 600, 800, 1000, and 1,200 °C

[affording materials identified as  $\text{SnO}_2(600)$ ,  $\text{SnO}_2(800)$ ,  $\text{SnO}_2(1000)$ , and  $\text{SnO}_2(1200)$ , respectively]. Figure 1 shows XRD patterns of the  $\text{SnO}_2$  materials.

**Figure 1.** XRD patterns of  $\text{SnO}_2$  materials calcined at (a) 600; (b) 800; (c) 1,000; and (d) 1,200 °C; ( $\blacklozenge$ )  $\text{SnO}_2$ .



Diffraction peaks were observed at 26.6, 33.8, 37.9, 51.8, 54.8, 61.9, 64.7, 65.9 and 71.3° 2 $\theta$ , and the intensities of these diffraction peaks increased with increasing temperature, indicating an increase in the crystallite size and the crystallinity [29,30], but the structures of  $\text{SnO}_2$  were retained. To confirm these results, the sizes of the  $\text{SnO}_2$  crystallites were calculated from the XRD patterns using Scherrer's equation Equation (3). As expected, the crystallite size of  $\text{SnO}_2$  increased from 19 to 54 nm with increasing calcination temperature (Table 1).

$$t = (K \cdot \lambda) / (W_{\text{size}} \cdot \cos \theta) = (0.9 \cdot \lambda) / (\text{FWHM} \cdot \cos \theta) \quad (3)$$

**Table 1.** Crystallite sizes calculated using XRD and TEM data.

$\text{SnO}_2$ materials	Wave Length (nm)	XRD			TEM	
		2 $\theta$ (°)	FWHM (cm <sup>3</sup> /g)	Crystallite Size (nm)	Crystallite Size (nm)	
$\text{SnO}_2(600)$	0.154	26.611	0.4095	19	10–20	
$\text{SnO}_2(800)$	0.154	26.581	0.3104	26	25–30	
$\text{SnO}_2(1,000)$	0.154	26.585	0.1690	47	40–50	
$\text{SnO}_2(1,200)$	0.154	26.604	0.1488	54	50–70	

In a separate experiment, TEM images of these  $\text{SnO}_2$  materials were investigated. Table 1 lists the crystallite sizes obtained from TEM images, which concur with those determined by XRD. Table 2

lists the textural properties of  $\text{SnO}_2$  materials, as determined by Hg porosimetry. The surface areas decreased with increasing calcination temperature, whereas the average pore diameters increased, presumably because the pore diameter is dependent on the crystallite size.

**Table 2.** Textural properties of the  $\text{SnO}_2$  materials produced by Hg porosimetry.

$\text{SnO}_2$ Materials	Surface Area ( $\text{m}^2/\text{g}$ )	Pore Volume ( $\text{cm}^3/\text{g}$ )	Average Pore Diameter (nm)
$\text{SnO}_2(600)$	24.8	0.4918	79
$\text{SnO}_2(800)$	16.4	0.5047	122
$\text{SnO}_2(1000)$	9.4	0.5226	222
$\text{SnO}_2(1200)$	8.0	0.6263	312

Figure 2 shows the response curves, responses and 80% response times of  $\text{SnO}_2(600)$ ,  $\text{SnO}_2(800)$ ,  $\text{SnO}_2(1000)$  and  $\text{SnO}_2(1200)$  gas sensors at a  $\text{H}_2\text{S}$  concentration of 1.0 ppm at 350 °C. The responses of the  $\text{SnO}_2$ -based sensors increased in the following order:  $\text{SnO}_2(600) < \text{SnO}_2(800) < \text{SnO}_2(1000) < \text{SnO}_2(1200)$ . The response time of the  $\text{SnO}_2(1200)$  sensor was much shorter than that of the  $\text{SnO}_2(600)$  sensor, even though sensor recovery was incomplete in air. These results mean that the response time decreases with increasing pore diameter, as shown in Table 1 and Figure 2(II), and the sensor response increases. However, the important point to note is the incomplete recovery of the sensors after the detection of  $\text{H}_2\text{S}$ , despite the high sensor response. It is thought that this result is because sulfur compounds are adsorbed on the sensor's surface, and that they progressively pollute the surface of tin dioxide.

**Figure 2.** (I) Response curves, (II) responses, and (II) 80% response times of  $\text{SnO}_2$ -based gas sensors, such as (a)  $\text{SnO}_2(600)$ ; (b)  $\text{SnO}_2(800)$ ; (c)  $\text{SnO}_2(1000)$ ; and (d)  $\text{SnO}_2(1200)$  at a  $\text{H}_2\text{S}$  concentration of 1.0 ppm at 350 °C.

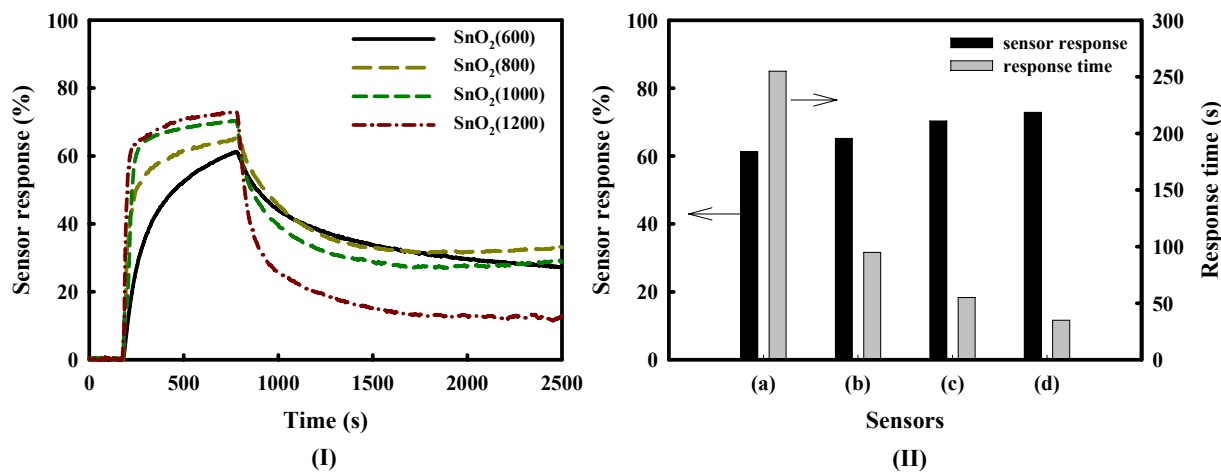
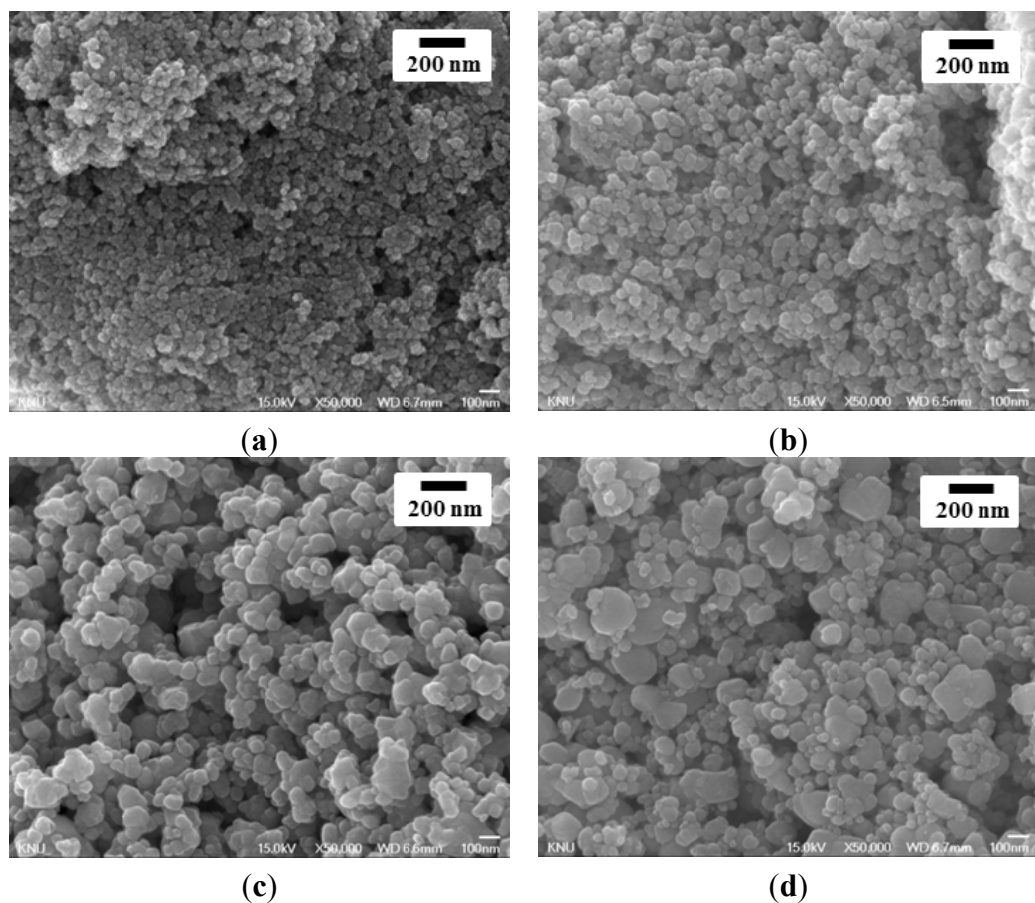


Figure 3 shows SEM images of the surfaces of the  $\text{SnO}_2(600)$ ,  $\text{SnO}_2(800)$ ,  $\text{SnO}_2(1000)$  and  $\text{SnO}_2(1200)$  thick-film sensors. The particle size of  $\text{SnO}_2$  increased with increasing calcination temperature in the following order:  $\text{SnO}_2(600) < \text{SnO}_2(800) < \text{SnO}_2(1000) < \text{SnO}_2(1200)$ . Liu *et al.* reported that the sensor sample based on  $\text{SnO}_2$  nanocrystals produced by the gel combustion method had higher response and shorter response times, which might be due to the more porous nano-crystallinity (~50 nm in size) than the sample prepared from hydrothermal-synthesized  $\text{SnO}_2$ .

nanocrystals, where smaller SnO<sub>2</sub> nanocrystals (~12–13 nm) are densely packed and agglomerate into large entities (secondary particles), approximately 2–3 μm in size [17]. However, in this study, particle size after screen-printing, as well as average pore diameter of SnO<sub>2</sub>, is directly related to the crystallite size (Table 1) and the crystallinity of SnO<sub>2</sub>, which is in contrast to Liu *et al.*'s results. This result is because the crystallite size and the crystallinity of SnO<sub>2</sub> was controlled by calcining the SnO<sub>2</sub> material, which was prepared by precipitation, at various temperatures (600, 800, 1,000 and 1,200 °C), and the SnO<sub>2</sub> thick-film sensors were fabricated on an alumina substrate by screen-printing using these calcined materials. From these results, it is clear that the sensor response and response time for the detection of H<sub>2</sub>S gas are directly affected by the SnO<sub>2</sub> pore diameter rather than to the surface area due to the diffusion of H<sub>2</sub>S gas. In particular, the important point to note is that the response time of the SnO<sub>2</sub> sensor, as well as sensor response for the detection of H<sub>2</sub>S, can be enhanced by increasing the crystallite size of SnO<sub>2</sub> by calcination.

**Figure 3.** SEM images of the SnO<sub>2</sub> thick-film sensors: (a) SnO<sub>2</sub>(600); (b) SnO<sub>2</sub>(800); (c) SnO<sub>2</sub>(1000); and (d) SnO<sub>2</sub>(1200).



### 3.2. Promoter Effects on Sensor Response and Recovery

The sensor recovery properties are an important consideration for sensors designed for H<sub>2</sub>S. To improve the sensor recovery, SnO<sub>2</sub>(1200)-based sensors were prepared by physically mixing with ZnO, Fe<sub>2</sub>O<sub>3</sub>, MoO<sub>3</sub>, NiO, or CuO promoters, which are referred to as Sn(12)Zn, Sn(12)Fe5, Sn(12)Mo5, Sn(12)Ni5, and Sn(12)Cu5, respectively. The effects of the promoters on the sensor

recovery properties were investigated at a H<sub>2</sub>S concentration of 1.0 ppm at 350 °C. The results obtained are summarized in Figure 4. The Sn(12)Zn5, Sn(12)Ni5 and Sn(12)Cu5 sensors showed a slight increase in the sensor response compared to the SnO<sub>2</sub> sensor, but their recoveries were incomplete at 350 °C. On the other hand, Sn(12)Fe5 and Sn(12)Mo5 showed complete recovery, but exhibited much lower responses than the SnO<sub>2</sub>(1200) sensor. In particular, the Sn(12)Mo5 sensor showed a faster recovery time than the Sn(12)Fe5 sensor, and a response that was approximately 42% higher than that of the SnO<sub>2</sub>(600)-based sensor containing 5 wt% MoO<sub>3</sub> [Sn(6)Mo5]. The reason for excellent recovery properties of the Fe5 and Mo5 sensors is not clear yet, but it is thought that Fe<sub>2</sub>O<sub>3</sub> and MoO<sub>3</sub> promoters added to SnO<sub>2</sub> play an important role in the desorption of sulfur compounds. To identify the effects of the promoters on the sensor response and recovery, the SnO<sub>2</sub>-based sensors promoted with various amounts of metal oxides (MoO<sub>3</sub>, NiO<sub>3</sub>, and ZnO) were examined at 1 ppm H<sub>2</sub>S and 350 °C. These results are shown in Figure 5. As shown by Figures 5(b,c) and (d), the Sn(12)Mo5 sensor achieved a recovery of 100%, even though the sensor response was decreased by the MoO<sub>3</sub> promoter. Previous studies found that NiO plays an important role in enhancing the sensor response of the SnO<sub>2</sub>-based sensor promoted with MoO<sub>3</sub> for the detection of dimethyl methylphosphonate (DMMP) and dichloromethane [23,24]. In the present study, the sensor response for the detection of H<sub>2</sub>S was increased by NiO (Figure 5). As expected, the Sn(12)Mo5Ni3 sensor, which was promoted with both MoO<sub>3</sub> and NiO, showed a sharp increase in the sensor response and maintained the sensor recovery properties (Figure 5(f)). In particular, the Sn(12)Mo5Ni3 sensor exhibited much higher sensor response and recovery than the Sn(6)Mo5Ni3 sensor [2] (39.2% and 91%, respectively). These results are attributed to diffusion effects caused by the larger pore size of SnO<sub>2</sub> and the promoter effects of NiO and MoO<sub>3</sub>. However, further study is required to verify the sensing mechanisms and the roles of NiO, ZnO, CuO, MoO<sub>3</sub>, and Fe<sub>2</sub>O<sub>3</sub> promoters in the sensor response and recovery properties.

**Figure 4.** Response curves of the SnO<sub>2</sub>-based gas sensors promoted with various metal oxides at a H<sub>2</sub>S concentration of 1.0 ppm at 350 °C.

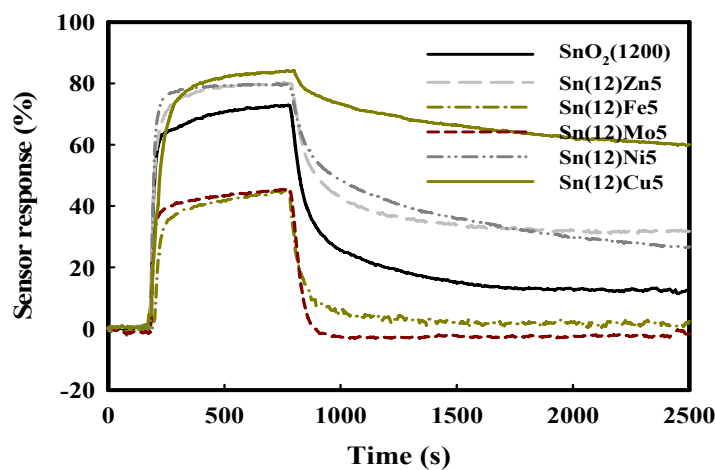


**Figure 5.** Responses and recoveries of the SnO<sub>2</sub>-based gas sensors promoted with various amounts of metal oxides at a H<sub>2</sub>S concentration of 1.0 ppm at 350 °C; (a) SnO<sub>2</sub>(1200); (b) Sn(12)Mo1; (c) Sn(12)Mo3; (d) Sn(12)Mo5; (e) Sn(12)Mo5Ni1; (f) Sn(12)Mo5Ni3; (g) Sn(12)Mo5Ni5; (h) Sn(12)Mo5Zn3; and (i) Sn(6)Mo5Ni3.

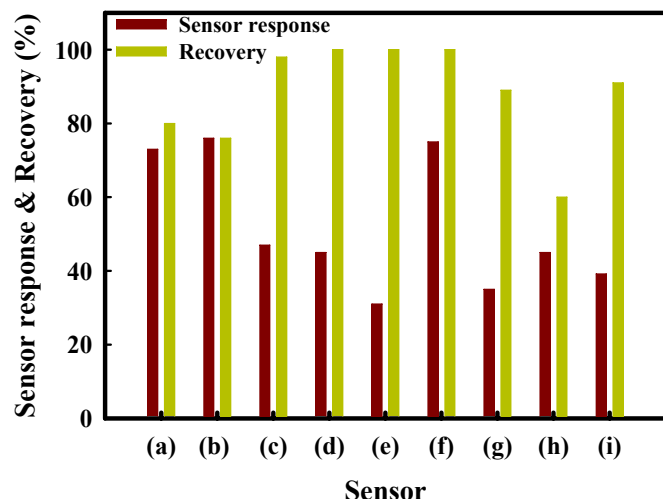


Figure 6 shows the response and recovery of the Sn(12)Mo5Ni3 sensor as a function of temperature at a H<sub>2</sub>S concentration of 1.0 ppm. The sensor response decreased slightly with increasing detection temperature, whereas the sensor recovery increased between 250 °C and 350 °C. Considering the sensor response and recovery, the optimum temperature for the detection of H<sub>2</sub>S was 350 °C.

**Figure 6.** Responses and recovery of the Sn(12)Mo5Ni3 sensor as a function of the detection temperature at a H<sub>2</sub>S concentration of 1.0 ppm.

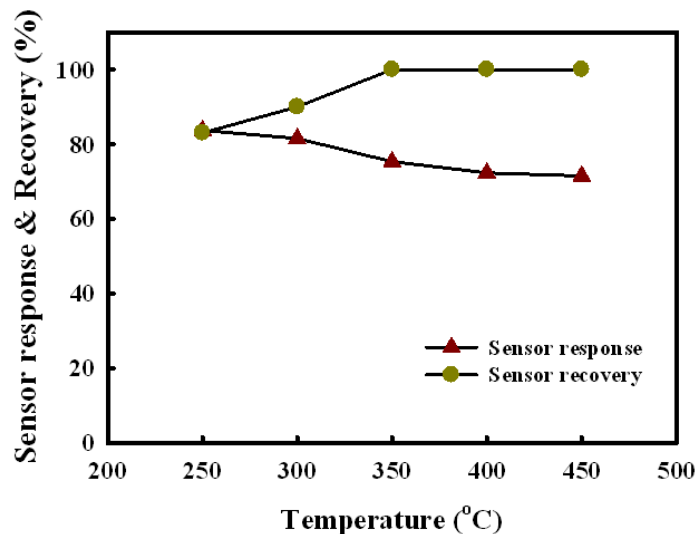


Figure 7 shows the response of the Sn(12)Mo5Ni3 sensor at concentrations between 0.25 ppm and 4 ppm at 350 °C. The response of this sensor increased almost linearly between 0.25 ppm and 4 ppm. The Sn(12)Mo5Ni3 sensor had a high sensor response of approximately 59% at low H<sub>2</sub>S concentrations of 0.25 ppm.

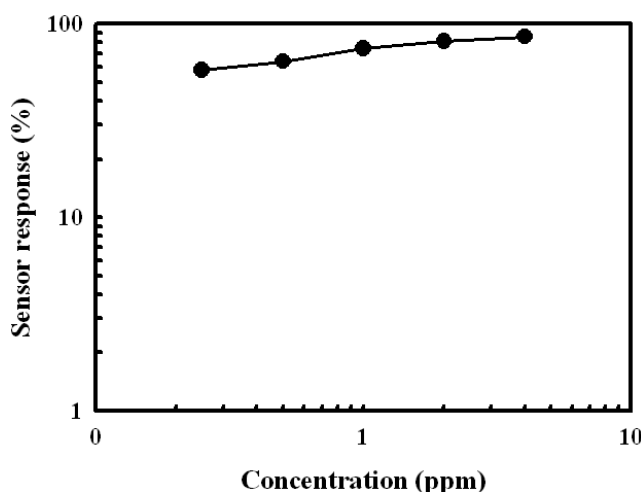
**Figure 7.** Response of the Sn(12)Mo5Ni3 sensor as a function of the H<sub>2</sub>S concentration.

Figure 8 shows the repeatabilities of the SnO<sub>2</sub>(1200), Sn(12)Mo5Ni3, and Sn(6)Mo5Ni3 sensors at a H<sub>2</sub>S concentration of 1 ppm and 350 °C. The response of the SnO<sub>2</sub>(1200) sensor decreased gradually over multiple detection and recovery tests. On the other hand, the Sn(12)Mo5Ni3 sensor maintained its response over multiple tests without deactivation. The response of the Sn(12)Mo5Ni3 sensor was approximately double that of the Sn(6)Mo5Ni3 sensor.

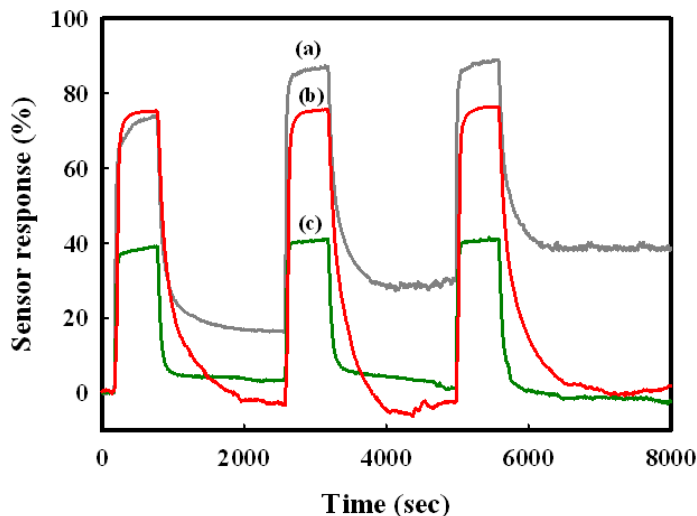
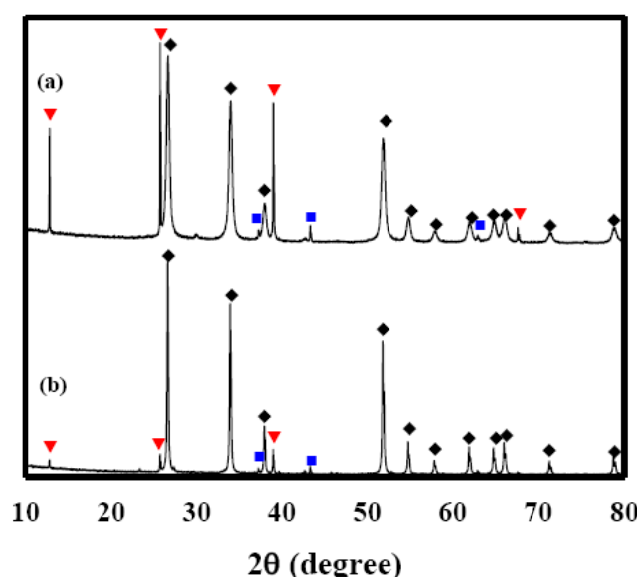
**Figure 8.** Repeatabilities of the (a) SnO<sub>2</sub>(1200); (b) Sn(12)Mo5Ni3; and (c) Sn(6)Mo5Ni3 sensors.

Figure 9 shows XRD patterns of Sn(6)Mo5Ni3 and Sn(12)Mo5Ni3 materials. Their XRD patterns showed MoO<sub>3</sub> (JCPDS No. 89-7112), NiO (JCPDS No. 89-7390) and SnO<sub>2</sub> (JCPDS No. 88-0287) phases. The diffraction peaks of these two materials were similar, as shown in Figure 9(a,b), which suggests that the observed enhancement in sensor response cannot be explained by structural differences alone. SEM images of the Sn(6)Mo5Ni3 and Sn(12)Mo5Ni3 sensors were observed at ×50 K and these results were shown in Figure 10. There is no change in the morphologies of those sensors as compared with the SnO<sub>2</sub>(600) and SnO<sub>2</sub>(1200) sensors. Table 3 lists the textural properties of the Sn(6)Mo5Ni3 and Sn(12)Mo5Ni3 materials determined by Hg porosimetry. The mean pore diameter of Sn(12)Mo5Ni3 was approximately double that of Sn(6)Mo5Ni3 (Table 3). This means that

the pore size of  $\text{SnO}_2$  and the promoter play important roles in the sensor response to  $\text{H}_2\text{S}$ . Based on these results, we believe that it is possible to prepare an excellent  $\text{SnO}_2$ -based sensor for the detection of  $\text{H}_2\text{S}$  at concentrations of < 1 ppm with a high sensor response and excellent recovery properties using  $\text{SnO}_2$  with a large pore size, in conjunction with  $\text{NiO}$  and  $\text{MoO}_3$  promoters.

**Figure 9.** XRD patterns of the (a)  $\text{Sn}(6)\text{Mo5Ni3}$  and (b)  $\text{Sn}(12)\text{Mo5Ni3}$  materials; (◆)  $\text{SnO}_2$ , (nO  $\text{MoO}_3$ ), and (nd  $\text{NiO}$ ).



**Figure 10.** SEM images of the (a)  $\text{Sn}(6)\text{Mo5Ni3}$  and (b)  $\text{Sn}(12)\text{Mo5Ni3}$  sensors.

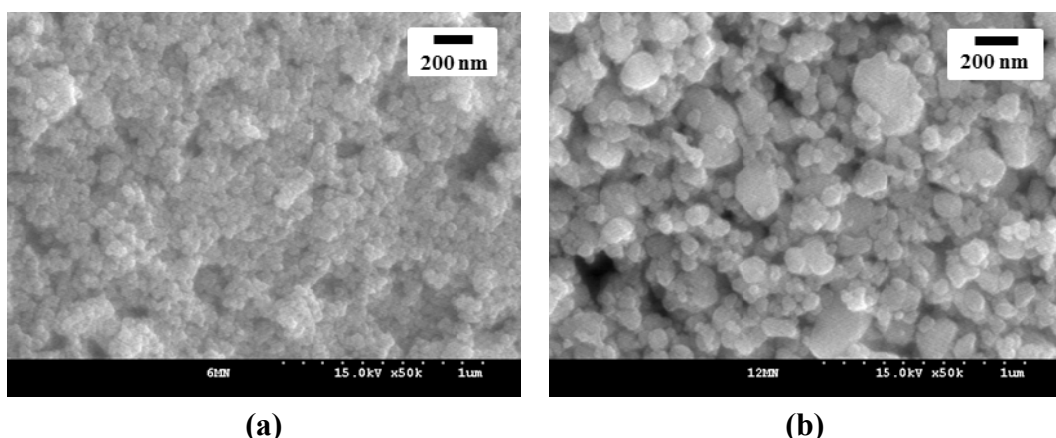


**Table 3.** Textural properties of the  $\text{Sn}(6)\text{Mo5Ni3}$  and  $\text{Sn}(12)\text{Mo5Ni3}$  by Hg porosimetry.

$\text{SnO}_2$ Materials	Surface Area ( $\text{m}^2/\text{g}$ )	Pore Volume ( $\text{cm}^3/\text{g}$ )	Average Pore Diameter (nm)
$\text{Sn}(6)\text{Mo5Ni3}$	11.8	0.5197	175.6
$\text{Sn}(12)\text{Mo5Ni3}$	4.7	0.4019	338.6

#### 4. Conclusions

A new large pore size  $\text{SnO}_2$ -based thick-film gas sensor promoted with  $\text{MoO}_3$  and  $\text{NiO}$  [ $\text{Sn}(12)\text{Mo5Ni3}$ ] was developed for the detection of  $\text{H}_2\text{S}$  at 350 °C. This sensor exhibited 100%

recovery at 350 °C and a maximum sensor response of 75%, and maintained a sensor response of 75% over many operating cycles without deactivation at a H<sub>2</sub>S concentration of 1 ppm and 350 °C. In addition, its response increased almost linearly between 0.25 and 1 ppm. Furthermore, the sensor exhibited a high response (59%) at a H<sub>2</sub>S concentration of only 0.25 ppm. In particular, the Sn(12)Mo5Ni3 sensor exhibited double the response of the corresponding Sn(6)Mo5Ni3 sensor, which was prepared by adding MoO<sub>3</sub> and NiO to SnO<sub>2</sub> calcined at 600 °C. These results are explained by the promoter effects of MoO<sub>3</sub> and NiO, and the diffusion effects associated with a large SnO<sub>2</sub> pore size.

## Acknowledgments

This work was supported by R&D program under Agency for Defense Development, Republic of Korea. We acknowledge the financial support by grants from Korea CCS R&D Center, funded by the Ministry of Education, Science and Technology of Korean government.

## References

1. Hwang, I.S.; Choi, J.K.; Kim, S.J.; Dong, K.Y.; Kwon, J.H.; Ju, B.K.; Lee, J.H. Enhanced H<sub>2</sub>S sensing characteristics of SnO<sub>2</sub> nanowires functionalized with CuO. *Sens. Actuators B* **2009**, *142*, 105–110.
2. Kim, S.Y.; Lee, S.C.; Hwang, B.W.; Lee, W.S.; Jung, S.Y.; Lee, D.D.; Kim, J.C. New SnO<sub>2</sub>-based thick film gas sensor promoted with molybdenum and nickel oxides for H<sub>2</sub>S detection. *J. Nanoelectron. Optoelectron.* **2011**, *6*, 293–296.
3. Jain, G.H.; Patil, L.A.; Wagh, M.S.; Patil, D.R.; Patil, S.A.; Amalnerkar, D.P. Surface modified BaTiO<sub>3</sub> thick film resistors as H<sub>2</sub>S gas sensors. *Sens. Actuators B* **2006**, *117*, 159–165.
4. Yamazoe, N.; Matsushima, S.; Maekawa, T.; Tamaki, J.; Miura, N. Control of Pd-dispersion in SnO<sub>2</sub> based sensors. *Meas. Sci. Technol.* **1991**, *1*, 201–205.
5. Gong, J.; Chen, Q.; Lian, M.; Liu, N.; Stevenson, R.G.; Adamic, F. Micromachined nanocrystalline silver doped SnO<sub>2</sub> H<sub>2</sub>S Sensor. *Sens. Actuators B* **2006**, *114*, 32149.
6. Lantto, V.; Romppainen, P. Response of some SnO<sub>2</sub> gas sensors to H<sub>2</sub>S after quick cooling. *J. Electrochem. Soc.* **1988**, *135*, 255055556.
7. Liu, J.H.; Huang, X.J.; Ye, G.; Liu, W.; Jiao, Z.; Chao, W.L.; Zhou, Z.; BYu, Z.L. H<sub>2</sub>S detection sensing characteristic of CuO/SnO<sub>2</sub> sensor. *Sensors* **2003**, *3*, 110–118.
8. Chowdhuri, A.; Gupta, V.; Sreenivas, K. Fast response H<sub>2</sub>S gas sensing characteristics with ultra-thin CuO islands on sputtered SnO<sub>2</sub>. *Sens. Actuator B* **2003**, *93*, 572–579.
9. Chowdhuri, A.; Gupta, V.; Sreenivas, K. Response speed of SnO<sub>2</sub>-based H<sub>2</sub>S gas sensors with CuO nanoparticles. *Appl. Phys. Lett.* **2004**, *84*, 1180–1182.
10. Kumar, R.; Khanna, A.; Tripathi, P.; Nandedkar, R.V.; Potdar, S.R.; Chaudhari, S.M.; Bhatti, S.S. CuO<sub>x</sub> element as hydrogen sulfide gas sensor prepared by a sequential electron beam evaporation technique. *J. Appl. Phys.* **2003**, *36*, 237737381.
11. Katti, V.R.; Debnath, A.K.; Muthe, K.P.; Kaur, M.; Dua, A.K.; Gadkari, S.C.; Gupta, S.K.; Sahni, V.C. Mechanism of drifts in H<sub>2</sub>S sensing properties of SnO<sub>2</sub>:CuO composite thin film sensors prepared by thermal evaporation. *Sens. Actuators B* **2003**, *96*, 2454052.

12. Yuanda, W.; Maosong, T.; Xiuli, H.; Yushu, Z.; Guorui, D. Thin film sensors of  $\text{SnO}_2\text{-nOsors}_{2,2}$  sandwich structure to  $\text{H}_2\text{S}$ . *Sens. Actuators B* **2001**, *79*, 1878091.
13. Patil, L.A.; Patil, D.R. Heterocontact type CuO-modified  $\text{SnO}_2$  sensor for the detection of a ppm level  $\text{H}_2\text{S}$  gas at room temperature. *Sens. Actuator B* **2006**, *120*, 316–323.
14. Wagh, M.S.; Patil, L.A.; Seth, T.; Amalnerkar, D.P. Surface cupricated  $\text{SnO}_2\text{-ZnO}$  thick film as a  $\text{H}_2\text{S}$  gas sensor. *Mater. Chem. Phys.* **2004**, *84*, 228–233.
15. Tsai, S.W.; Chiou, J.C. Improved crystalline structure and  $\text{H}_2\text{S}$  sensing performance of CuO-Au- $\text{SnO}_2$  thin film using  $\text{SiO}_2$  additive concentration. *Sens. Actuators B* **2011**, *152*, 176–182.
16. Park, H.D.; Lee, D.D.; Lee, W.I.; Kim, J.M.; Kim, J.M. Sensitivity of  $\text{SnO}_2$ -based thick-film devices to  $\text{CH}_3\text{CN}$ . *Sensor. Meter.* **1994**, *5*, 209–220.
17. Liu, H.; Gong, S.P.; Hu, Y.X.; Liu, J.Q.; Zhou, D.X. Properties and mechanism study of  $\text{SnO}_2$  nanocrystals for  $\text{H}_2\text{S}$  thick-film sensors. *Sens. Actuator B* **2009**, *140*, 190–195.
18. Brunol, E.; Berger, F.; Fromm, M.; Planade, R. Detection of dimethyl methylphosphonate (DMMP) by tin dioxide-based gas sensor: Response curve and understanding of the reactional mechanism. *Sens. Actuator B* **2006**, *120*, 35–41.
19. Berger, F.; Brunol, E.; Planade, R.; Chambaudet, A. Detection of DEMP vapors using  $\text{SnO}_2$ -based gas sensors: Understanding of the chemical reactional mechanism. *Thin Solid Films* **2003**, *436*, 136.
20. Choi, N.J.; Lee, Y.S.; Kwak, J.H.; Park, J.S.; Park, K.B.; Shin, K.S.; Park, H.D.; Kim, J.C.; Huh, J.S.; Lee, D.D. Classification of chemical warfare agents using thick film gas sensor array. *Sens. Actuators B* **2005**, *108*, 298–304.
21. Kim, J.C.; Jun, H.K.; Huh, J.S.; Lee, D.D. Tin oxide-based methane gas sensor promoted by alumina-supported Pd catalyst. *Sens. Actuators B* **1997**, *45*, 271–277.
22. Lee, W.S.; Lee, S.C.; Lee, S.J.; Lee, D.D.; Huh, J.S.; Jun, H.K.; Kim, J.C. The sensing behavior of  $\text{SnO}_2$ -based thick-film gas sensors at a low concentration of chemical agent simulants. *Sens. Actuators B. Chem.* **2005**, *108*, 148–153.
23. Lee, W.S.; Choi, H.Y.; Lee, S.C.; Lee, S.J.; Lee, D.D.; Huh, J.J.; Kim, J.C. Recoverable  $\text{SnO}_2$ -based sensors promoted with  $\text{MoO}_3$  and  $\text{Sb}_2\text{O}_3$  for the detection of DMMP. *Rare Met. Mater. Eng.* **2006**, *35*, 155–156.
24. Lee, S.C.; Hwang, B.W.; Lee, S.J.; Choi, H.Y.; Kim, S.Y.; Jung, S.Y.; Ragupathy, D.; Lee, D.D.; Kim, J.C. A novel tin oxide-based recoverable thick film  $\text{SO}_2$  gas sensor promoted with magnesium and vanadium oxides. *Sens. Actuators B* **2011**, *160*, 1328–1334.
25. Lee, S.C.; Kim, S.Y.; Lee, W.S.; Jung, S.Y.; Hwang, B.W.; Ragupathy, D.; Lee, D.D.; Lee, S.Y.; Kim, J.C. Effects of textural properties on the response of a  $\text{SnO}_2$ -based gas sensor for the detection of chemical warfare agents. *Sensors* **2011**, *11*, 6893–6904.
26. Lee, S.C.; Choi, H.Y.; Lee, S.J.; Lee, W.S.; Huh, J.S.; Lee, D.D.; Kim, J.C. The development of  $\text{SnO}_2$ -based recoverable gas sensors for the detection of DMMP. *Sens. Actuators B* **2009**, *137*, 239–245.
27. Lee, S.C.; Choi, H.Y.; Lee, S.J.; Lee, W.S.; Huh, J.S.; Lee, D.D.; Kim, J.C. Novel  $\text{SnO}_2$ -based gas sensors promoted with metal oxides for the detection of dichloromethane. *Sens. Actuators B* **2009**, *138*, 446–452.

28. Lee, S.C.; Choi, H.Y.; Lee, W.S.; Lee, S.J.; Ragupathy, D.; Lee, D.D.; Kim, J.C. Improvement of recovery of SnO<sub>2</sub>-based thick film gas sensors for dimethyl methylphosphonate (DMMP) detection. *Sens. Lett.* **2011**, *9*, 101–105.
29. Lu, C.H.; Yeh, C.H. Influence of hydrothermal conditions on the morphology and particle size of zinc oxide powder. *Ceram. Int.* **2000**, *26*, 351–357.
30. Chena, Y.F.; Lee, C.Y.; Yeng, M.Y.; Chiu, H.T. The effect of calcination temperature on the crystallinity of TiO<sub>2</sub> nanopowders. *J. Cryst. Growth* **2003**, *247*, 363–370.

© 2013 by the authors; licensee MDPI, Basel, Switzerland. This article is an open access article distributed under the terms and conditions of the Creative Commons Attribution license (<http://creativecommons.org/licenses/by/3.0/>).